Influence of crystallographic orientation on the recrystallization of pure tantalum through microstructure-based estimation of the stored energy

J. Baton, W. Geslin, Charbel Moussa

Influence of crystallographic orientation on the recrystallization of pure tantalum through microstructure-based estimation of the stored energy

J. BATON[a, *], W. GESLIN[b], C. MOUSSA[a]

[a]MINES ParisTech, PSL Research University, CEMEF - Centre de mise en forme des matériaux, CNRS UMR 7635, CS 10207 rue Claude Daunesse, 06904 Sophia Antipolis Cedex, France

[b]CEA DAM Valduc, F-21120 Is-sur-Tille, France

* Corresponding author.

E-mail address: jules.baton@laposte.net (J. Baton).

Abstract

Plastic deformation and static recrystallization of pure tantalum are studied using Electron BackScatter Diffraction (EBSD) technique. Recrystallization kinetics are discussed in light of stored energy estimation from EBSD data acquired on deformed microstructures. Characterization of deformed state reveals the influence of crystallographic orientation on the plastic deformation. Dislocation substructures are formed in the γ-fiber grains and almost no substructures are observed in the θ-fiber grains. Subsequent recrystallization directly inherits this orientation dependence of deformed state. Nucleation is promoted in the γ-fiber grains because of substructure development whereas nucleation is more sluggish to occur in the θ-fiber grains. Thus, a microstructure composed mostly of γ-fiber grains recrystallizes faster than a microstructure with a less strong texture, despite a strain nearly three times lower. At the polycrystalline scale (step size of 1.20 µm in the present case), recrystallization kinetics are better described with stored energy estimated through substructures than through dislocation density. At the substructure scale (step size of 90 nm), Geometrically Necessary Dislocation (GND) density seems to be correctly estimated; still recrystallization kinetics cannot be accounted for by this density because it does not account for the substructure formation.

Keywords

Tantalum; Dislocation substructures; Stored energy; Crystallographic orientation; Recrystallization; EBSD

1. Introduction

Tantalum is a body centered cubic (bcc) metal with a high melting temperature (T_m = 2996°C) used for several industrial applications such as chemical processing, military or electronic applications [1]. It is a very ductile metal at room temperature, which enables the cold forming of parts with intricate shapes. Dislocations created during cold deformation are the stored energy that constitutes the driving force for thermally activated recovery and recrystallization during subsequent annealing.

The crystallographic orientation affects significantly the plastic deformation of grains and the development of dislocation substructures as observed on face centered cubic (fcc) [2] and bcc [3,4] metallic alloys. This influence leads to an orientation dependence of the stored energy. For instance, it was often observed on rolled bcc metals that the stored energy was higher in the grains with the direction <111> parallel to the normal direction of the sheet than in the other grains [3,5]. Thus, this orientation dependence has direct consequences on subsequent recrystallization. Indeed, as observed on tantalum, nucleation is favored in grains forming substructures and growth occurs faster in grains with high stored energy as observed on tantalum [6,7] and on molybdenum [8] for instance.

The stored energy can be estimated with several methods at different scales of characterization such as calorimetry [9], X-ray diffraction [10], Transmission Electron Microscopy (TEM) [11] and Scanning Electron Microscopy (SEM) with Electron BackScatter Diffraction (EBSD) [12,13]. For the latter method with EBSD, intragranular disorientation is used to assess the stored energy mainly through two approaches. In the first approach, it is assumed that most of dislocations form subboundaries. Hence, the stored energy is the sum of the energies of all the subboundaries estimated depending on their disorientation with the Read-Shockley model [14]. A detailed description can be found in [15]. In the second approach, the stored energy is estimated through the dislocation density estimated from EBSD data [11,16]. These two approaches are detailed in section 6.

Bulk and local stored energies, estimated by calorimetry and microstructural measurements respectively, were compared in several studies performed on aluminum [17], copper [18], nickel [19] and interstitial free steel [20]. Similar qualitative trends were generally observed

but quantitatively, the bulk stored energy was always higher than the local stored energy. This underestimation with the microscopic approaches, performed with TEM or EBSD, is probably because some of the dislocations (Statistically Stored Dislocations, SSDs) are not assessed with microscopy. Moreover, when the measurements are done from EBSD data, the angular resolution of the technique and the use of angular thresholds for the determination of subboundaries are another cause for this underestimation.

The aim of the present investigation is to analyze the recrystallization behavior of pure tantalum through the estimation of the stored energy. Compressed and rolled samples with different initial texture were annealed in order to study the influence of crystallographic orientation on recrystallization. Recrystallized microstructures were characterized using the EBSD technique through the recrystallized fraction, size and orientation of recrystallized grains. The differences of recrystallization behavior between the compression case and the rolling case are discussed. Estimations of the stored energy through dislocation densities and substructure measurements are compared in light of a better description of the deformed state.

2. Characterization conditions

A Zeiss Supra40 Field Emission Gun Scanning Electron Microscope (FEG-SEM) operated at 20 kV was used in order to acquire EBSD orientation maps. This microscope is equipped with a Bruker Quantax system that contains a FlashHR EBSD detector and is controlled by the Esprit 2.1 EBSD software. The sample preparation procedure is detailed in [3]. Two scales of characterization were used in this study. For characterization at the polycrystalline scale, the acquisitions were carried out with a compromise between the spatial resolution and the statistical representativeness of the observed area with a step size of 1.20 µm over a grid of 1.20 mm × 0.90 mm. For characterization at the substructure scale, a step size of 90 nm was chosen and EBSD maps were carried out far from grain boundaries. EBSD data post-treatments were done using the MTEX toolbox available on Matlab® [21].

3. Material and experimental conditions

Pure tantalum (> 99.99% wt.) was received as a 12 mm thick sheet formed by cold rolling and then annealed in order to have a fully recrystallized microstructure. Samples were taken from

the mid-thickness and quarter-thickness (3 mm from the center). The corresponding EBSD maps of the initial state, presented in Fig.1a and 2a, show fully recrystallized microstructures. The main difference between them is the crystallographic orientation of grains. In order to analyze this difference, grains were sort into three classes depending on their mean orientations: grains of the θ-fiber for which the direction <100> is parallel to the normal direction of the sheet (ND), grains of the γ-fiber for which the direction <111> is parallel to ND and grains of the class "Other" are the ones that do not belong to either of the two previous fibers. For further details concerning the θ and γ-fibers texture components the reader is invited to see Fig.2c in [3], where those texture components are explicitly presented in the Orientation Distribution Function (ODF) with their location in terms of Euler angles. The above mentioned classification was carried out with a tolerance of 15°. A disorientation angle threshold of 10° was used for the determination of grain boundaries. The γ-fiber is very predominant (≈ 80%) at the center of the sheet (Fig.1a). In contrast, orientations are more homogeneously distributed in the quarter layer (Fig.2a) with mostly "other" orientations (≈ 57%) and lower θ-fiber (≈ 33%) and γ-fiber (≈ 10%) content.

Compression tests were carried out at room temperature on samples taken from the entire thickness of the sheet (initial state presented in Fig.1a) for a von Mises equivalent strain of $\varepsilon_{VM} \approx 0.65$. Details on the deformation conditions can be found in [3]. The Compression Direction CD was chosen parallel to ND. The corresponding microstructure is presented in Fig.1b. Cold rolling was also used for plastic deformation on samples taken from one half of the sheet (initial state presented in Fig.2a) for a total reduction of 76% and a corresponding equivalent strain of $\varepsilon_{VM} \approx 1.67$. Microstructure was observed in the central region of the samples, where it can be considered that plane strain is taking place and that the effect of shear near surface region is negligible. Details on the deformation conditions can be found in [3]. The Normal Direction ND of the rolling is parallel to the one of the initial sheet. The corresponding microstructure is presented in Fig.2b.

The influence of the deformation mode is out of the scope of this work. All the observations are discussed regarding the difference in texture between the two initial states and not regarding the difference in the deformation mode. The two cases are nevertheless distinguished by "Compression" and "Rolling" in order to facilitate the presentation of the results.

The deformed samples were annealed at high vacuum (pressure around 10^{-2} Pa) at 850°C with a heating rate of around 20°C/min for three different holding times: 1h, 2h and 3h. Air cooling was applied at the end of the treatment.

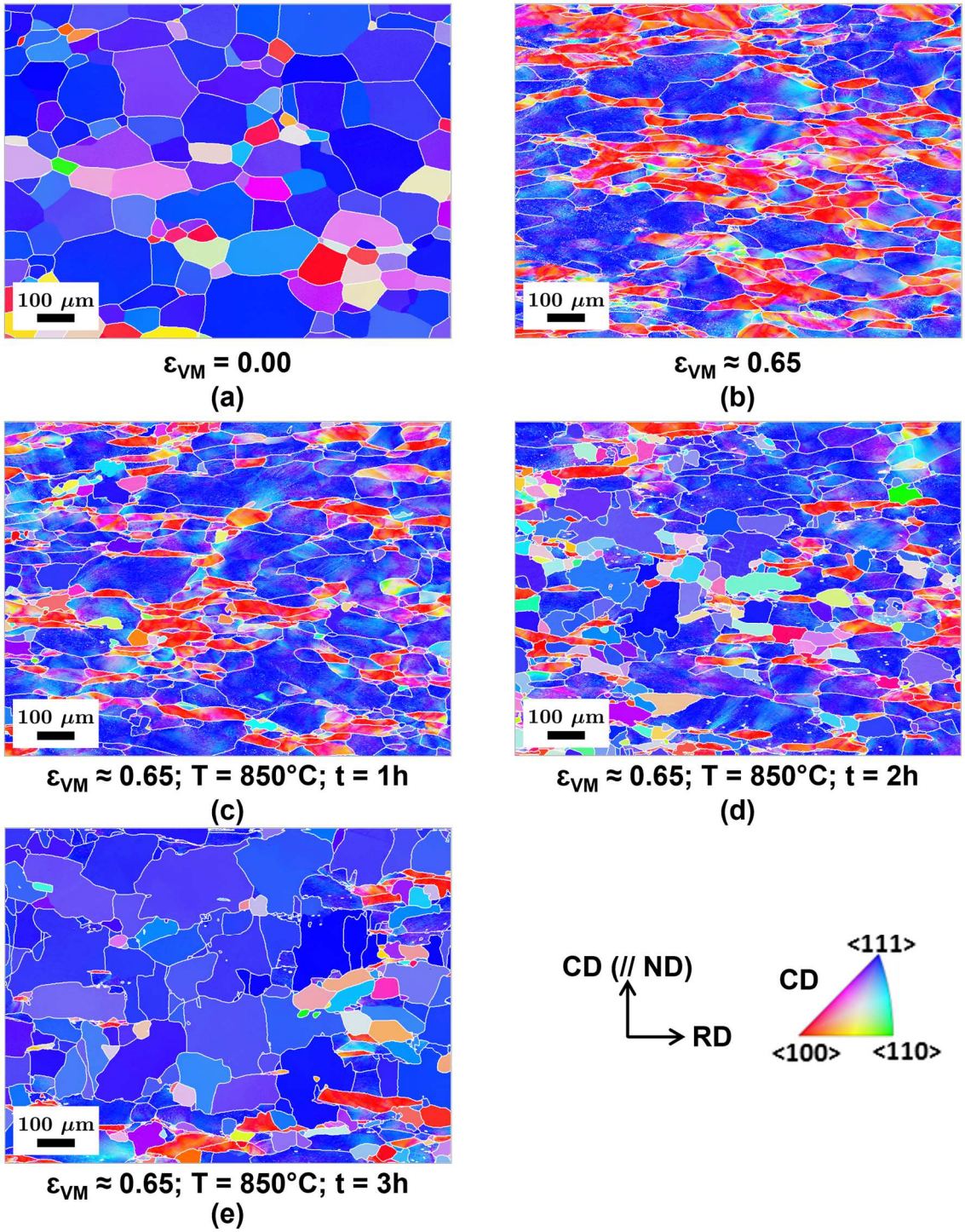

Fig.1 EBSD orientation maps of (a) the center of the as-received sheet, (b) the compressed sample for $\varepsilon_{VM} \approx 0.65$ and the annealed samples at 850°C for (c) 1h, (d) 2h and (e) 3h.

(Normal Direction ND projected onto the standard triangle; RD stands for Radial Direction). Grain boundaries are plotted in white lines. Fig.1a and 1b from [3].

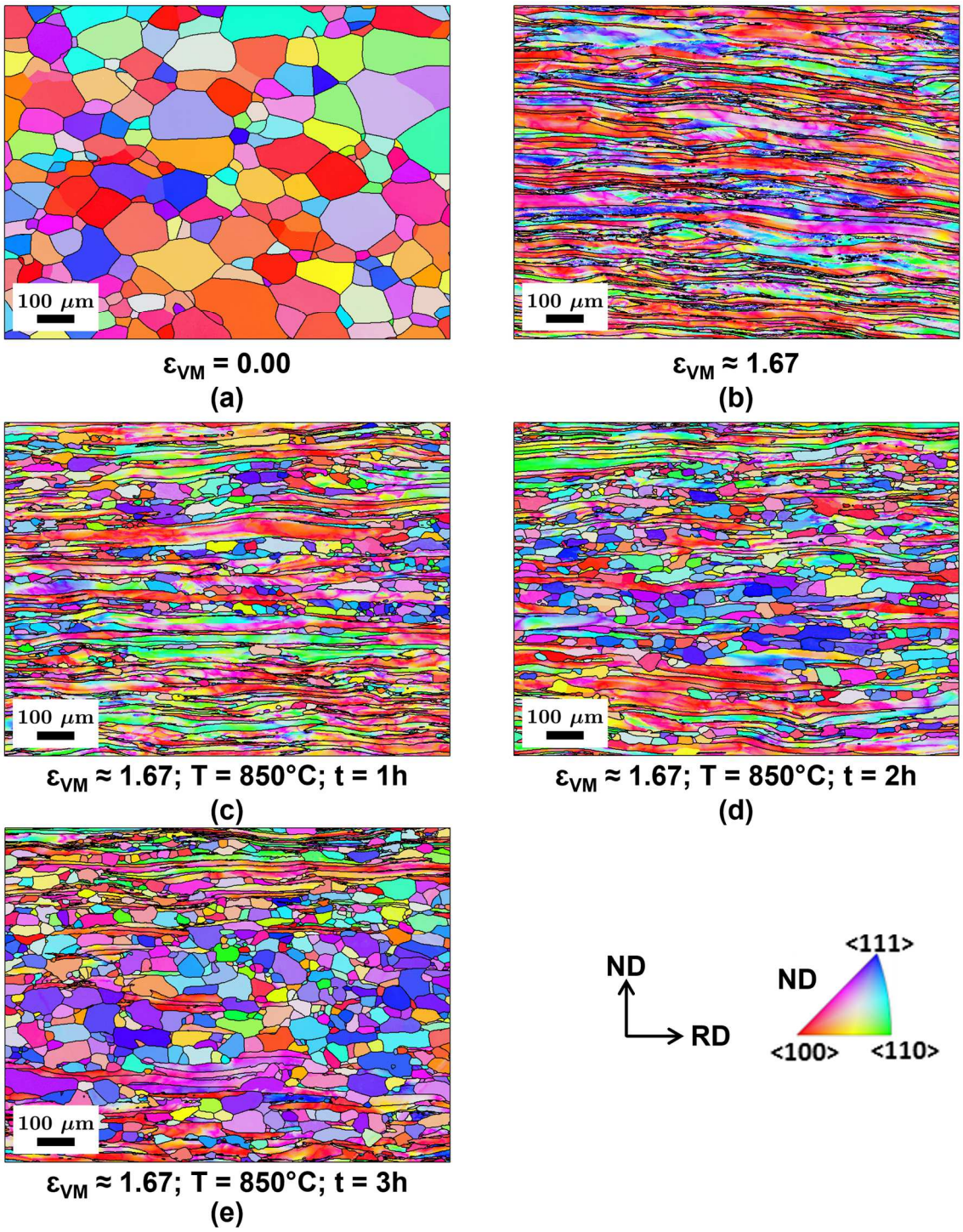

Fig.2 EBSD orientation maps of (a) the quarter layer of the as-received sheet, (b) the rolled sample for $\varepsilon_{VM} \approx 1.67$ and the annealed samples at 850°C for (c) 1h, (d) 2h and (e) 3h. (ND

projected onto the standard triangle; RD stands for Rolling Direction). Grain boundaries are plotted in black lines. Fig.2a and 2b from [3].

4. Deformed microstructures

A detailed analysis of the microstructural evolutions during plastic deformation is presented in a previous study [3]. Only the results necessary for the recrystallization analysis are reported here. For additional discussion on deformation (and recrystallization) bcc texture, the reader can refer to [22,23].

Dislocation density can be estimated from EBSD data through disorientations [12,13]. However, it is admitted that this estimation is scale dependent. Thus, the dislocation densities estimated from EBSD data are defined as ρ_{EBSD} in order to avoid employing a physically based definition (generally Geometrically Necessary Dislocations, GNDs term is used) for a parameter which depends on the scale of observation [3,7].

In order to estimate ρ_{EBSD}, the formalism proposed by Pantleon [24] and its implementation with the MTEX toolbox [21] realized by Seret et al. [25] was used.

Average value of ρ_{EBSD} ($\overline{\rho_{EBSD}}$) obtained for the two studied strains are presented in Table 1. The dislocation content is higher for the rolling case, which is in agreement with a higher strain. Besides, the influence of the crystallographic orientation on the deformation can be investigated by calculating $\overline{\rho_{EBSD}}$ for each class of orientations. This calculation was performed for the rolling case only, as the texture of the compression case is mostly composed of γ-fiber grains. Results, presented in Table 1, show that $\overline{\rho_{EBSD}}$ is lower for the θ-fiber grains compared with the γ-fiber grains. $\overline{\rho_{EBSD}}$ of "other" grains lies between the ones of the two other classes of grains. This trend has been confirmed for different strains [3] and is in accordance with previous studies on cold rolled pure tantalum [9,26].

Deformed microstructures presented in Fig.1b and 2b were characterized at a lower scale with EBSD maps with a step size of 90 nm in order to quantify the development of dislocation substructures. For that purpose, EBSD maps were acquired in several grains for each strain studied and each class of orientations (only the γ-fiber grains were considered for the compression case). The reader is invited to report to the previous study [3] for detailed statistics on the number of grains in which EBSD maps were acquired and the corresponding total examined area. In this work, all the segments between neighboring pixels with a disorientation angle between 1.5° and 10° were regarded as subboundaries and quantified

through two parameters [3,7]. The first one, $\overline{\theta_{sub}}$, is the mean disorientation angle of subboundaries. The second one, $\overline{\rho_{sub}^{l}}$, is the total subboundary length divided by the total examined area.

The two parameters were calculated for each case and results are presented in Table 1. Dislocation substructures are more developed in the γ-fiber grains than in the two other classes of grains for the rolling case. The number of subboundaries in the γ-fiber grains is the same for the rolling case and the compression case indicating a faster development with strain for the compression case. This difference is due to the difference in texture between the two initial states [3], the initial microstructure for compression being composed of around 80% of γ-fiber grains and presenting a more homogeneous development of subboundaries in the microstructure. Moreover, the comparison between the θ-fiber grains and the "other" grains highlights that the characterization of deformed state is not straightforward. Indeed, even though the dislocation density at the polycrystalline scale in the "other" grains is higher than in the θ-fiber grains, the substructure development is rather equivalent between the two cases. This observation questions the correct method to estimate the stored energy and will be further discussed in section 6.

Table 1 Quantitative characterization of deformed samples at the polycrystalline scale ($\overline{\rho_{EBSD}}$) and at the substructure scale ($\overline{\theta_{sub}}$, $\overline{\rho_{sub}^{l}}$). Data from [3].

Deformation condition	Class of orientations	$\overline{\rho_{EBSD}}$ (m^{-2})	$\overline{\theta_{sub}}$ (°)	$\overline{\rho_{sub}^{l}}$ (μm^{-1})
Compression $\varepsilon_{VM} \approx 0.65$	All gathered	1.1×10^{15}	/	/
	γ-fiber	1.0×10^{15}	2.8	1.7
Rolling $\varepsilon_{VM} \approx 1.67$	All gathered	1.8×10^{15}	/	/
	θ-fiber	1.4×10^{15}	2.7	0.23
	γ-fiber	2.3×10^{15}	3.6	1.7
	"Other" class	2.0×10^{15}	2.8	0.23

5. Recrystallized microstructures

5.1. Microstructural evolutions with annealing time

EBSD maps of samples after annealing at 850°C for 1h, 2h, and 3h are presented in Fig.1c, 1d and 1e for the compression case and in Fig.2c, 2d and 2e for the rolling case respectively. For each case, the recrystallized fraction was quantified through the Grain Average Misorientation (GAM) and the Grain Orientation Spread (GOS). For that purpose, the distributions of these two parameters were used to estimate a threshold ($0.6° \pm 0.2°$ for GAM and $0.8° \pm 0.2°$ for GOS) for separating the recrystallized grains with low values and the non-recrystallized grains with high values. Once the recrystallized grains were determined, their size was calculated. To do so, grains smaller than five pixels or on the edges of EBSD maps were excluded from the analysis. Then, the size (considered as the equivalent diameter) of each grain was calculated. The mean grain size was determined as the surface weighted average of grain sizes.

The evolution of the recrystallized fraction and of the mean grain size with annealing time are presented in Fig.3a and 3b for the two studied cases. As expected, the recrystallized fraction increases with annealing time for both cases. However, it can be observed that the compressed sample recrystallized after 2h as much as the rolled sample despite a strain nearly three times lower and a lower dislocation density at the polycrystalline scale (Table 1). This demonstrates that the macroscopic strain and $\overline{\rho_{EBSD}}$ are not relevant to correctly predict recrystallization. This observation will be further discussed in section 6.

The higher recrystallized grain size in the compression case compared to in the rolling case can be explained by a higher number of recrystallized grains in the latter case. Indeed, the increase in the total grain boundary length due to the higher plastic deformation (Fig.2b) implies an increase in the number of potential nucleation sites. In addition, it can be noticed that the increase of recrystallized grain size with time is faster in the compression case than in the rolling case. The fast increase of recrystallized fraction and the slow increase of recrystallized grain size for the rolling case is an indicator of a continuous nucleation process all along the annealing and a dominance of nucleation on growth. At the opposite, nucleation seems to occur mainly at the early stages of annealing for the compression case. In addition to the highest number of grain boundaries in the rolling case previously mentioned, this nucleation process is directly inherited from the deformed microstructures. As previously demonstrated [3], dislocation substructures develop in a homogeneous way when the number of γ-fiber grains is dominant. An indication for this was a fast increase of the number of

subboundaries through $\overline{\rho_{sub}^{l}}$ since the early stages of deformation and then a saturation for $\varepsilon_{VM} > 0.65$. For higher strains, only the disorientation of the subboundaries increased but not their quantity. For the rolling case, where the texture of the initial microstructure is less pronounced, the number of dislocation subboundaries increased continuously up to $\varepsilon_{VM} \approx 1.67$ without any saturation. Hence for the compression case, where the γ-fiber grains are dominant, the nucleation occurs almost simultaneously in all the microstructure because of this homogeneous distribution, which is not the case for the rolling case.

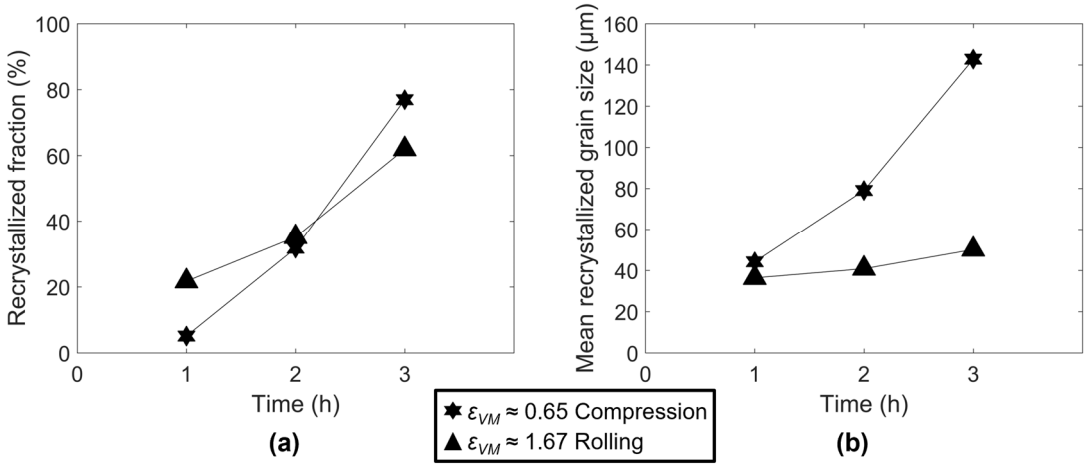

Fig.3 Evolution of (a) the recrystallized fraction and (b) the mean recrystallized grain size with annealing time for the two studied strains.

5.2. Influence of crystallographic orientation on recrystallization

The evolution of the surface fraction of recrystallized grains for each class of orientations with annealing time are presented in Fig.4a and 4b for the compression case and the rolling case respectively. For both cases, most of the recrystallized grains belong to the γ-fiber or to the "other" class. This composition of the texture is necessarily related to the differences inherited from the deformed state [7]. Nucleation is enhanced in the γ-fiber deformed grains due to a more advanced substructure development in comparison with the other grains for a given strain. Conversely, nucleation is more sluggish in the θ-fiber deformed grains and these grains are more susceptible to being consumed by growth of surrounding recrystallized grains than by nucleation of θ-fiber recrystallized grains. In addition, the faster evolution of γ-fiber recrystallized grain fraction for the compression case demonstrates a faster growth for this class of grains. The higher fraction of γ-fiber grains at the deformed state in the compression case than in the rolling case explains the higher fraction of γ-fiber recrystallized grains in the

former case. An additional important conclusion is that this high fraction of γ-fiber recrystallized grains is an indicator that the crystallographic orientation of recrystallized grains is inherited from the deformed state.

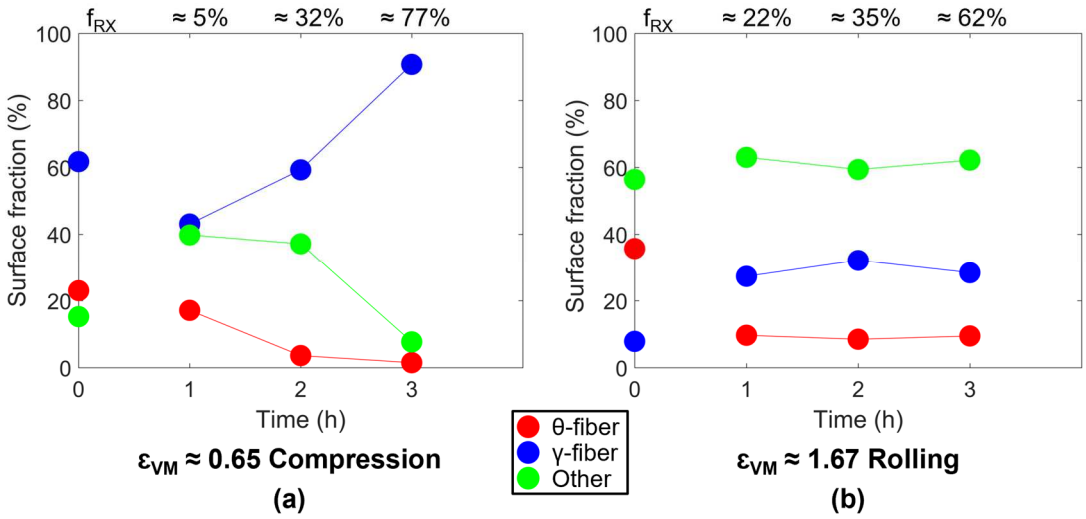

Fig.4 Evolution of the surface fraction of recrystallized grains for each class of orientations with annealing time for (a) the compression case and (b) the rolling case. Surface fractions at the deformed state indicated at time 0h. The recrystallized fractions f_{RX} for all the cases are on the top of the figures.

The evolution of the size of the recrystallized grains for each class of orientations with annealing time are presented in Fig.5a and 5b for the compression case and the rolling case respectively. It can be noted that the crystallographic orientation of deformed grains has also an influence on the size of recrystallized grains. Indeed, the size of γ-fiber recrystallized grains is higher than the one of the other grains. This size advantage can be explained by a shorter incubation time for nucleation, resulting from the more completed development of substructures in the γ-fiber deformed grains than in the others [7].

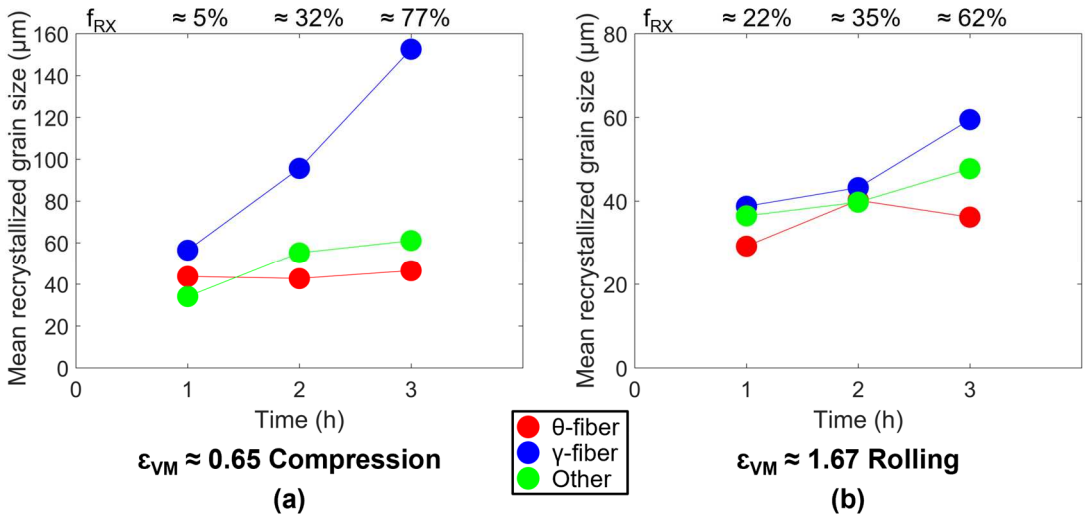

Fig.5 Evolution of the mean recrystallized grain size for each class of orientations with annealing time for (a) the compression case and (b) the rolling case.

6. Estimation of the stored energy

Methods presentation

Results presented in section 5 highlight that the compressed sample recrystallized faster than the rolled sample despite a strain three times lower. This difference can presumably be explained by the more developed substructures in the compression case (composed mostly of γ-fiber grains), which enhances nucleation and thus recrystallization. Stored energy is one of the parameters to consider in order to better quantify these differences. In the present work, two methods were employed in order to estimate the stored energy from EBSD data: one based on dislocation density and one based on dislocation substructures. A reminder of these two methods is given in the following.

In the first method, based on the dislocation density, the total stored energy is considered to be the sum of the energy of each dislocation taken individually. A value of stored energy can then be estimated from a dislocation density [11]:

$$E \approx C\rho G b^2 \quad (1)$$

where E is the total stored energy (J/m^3), $C = 0{,}5$ is a constant ($\approx$ 0,5 – 1 [16]), ρ is the dislocation density (m^{-2}), G is the shear modulus (69×10^9 N/m^2 for tantalum) and b is the norm of the Burgers vector (2.86×10^{-10} m for tantalum).

The major drawback of this method is that the interactions between dislocations are only considered in an approximate way [16]. Indeed, the elastic strain fields around the dislocations interact and compensate each other. These interactions, which are the highest when dislocations form subboundaries, result in a lower dislocation energy [11]. Furthermore, the disorientations detected by EBSD are those caused by dislocations which have a cumulative effect (i.e. GNDs or a part of them depending on the step size) and not by dislocations with a cumulative effect leading to very low disorientations. Thus, the basic assumption of equation (1) lies in opposition to the nature of the dislocations detected by EBSD.

In the second method, based on the energy of subboundaries, all the dislocations are grouped into subboundaries and thus the total stored energy is considered to be the sum of the energy of each subboundary. It can be estimated as:

$$E \approx E_{subboundaries} \approx \gamma_{sub} S_{sub} \qquad (2)$$

where γ_{sub} is the energy of subboundaries (J/m^2) and S_{sub} is the total surface of subboundary per unit volume (m^2/m^3). The energy of subboundaries can be estimated by the Read-Shockley model [14]:

$$\gamma_{sub} = \gamma_{GB} \frac{\theta_{sub}}{\theta_{GB}} (1 - \ln \frac{\theta_{sub}}{\theta_{GB}}) \qquad (3)$$

where γ_{GB} is the energy of grain boundaries ($\approx$ 1.2 J/m^2 for tantalum [27]), θ_{sub} is the disorientation angle of subboundaries and θ_{GB} is the angular limit value of disorientation to define a grain boundary (10° in the present case).

The stored energy is calculated for each segment corresponding to a subboundary. Thus, the total stored energy is the sum of the contribution of each segment of all the subboundaries:

$$E = \sum_i^N E_i = \sum_i^N \gamma_{sub}(\theta_i)\, S_{sub_i} \qquad (4)$$

where N is the total number of segments, $\gamma_{sub}(\theta_i)$ is the energy of each segment and S_{sub_i} is the surface per unit volume of each segment. As the EBSD maps were acquired on square grids, S_{sub_i} can be written as:

$$S_{sub_i} = \frac{4}{\pi} \cdot \frac{\pi}{4} \cdot \frac{\Delta}{S} = \frac{\Delta}{S} \qquad (5)$$

where Δ is the step size (m), S is the total examined area with EBSD (m^2), $\pi/4$ is a corrective factor used to consider the overestimation caused by the discrete grid [28] and $4/\pi$ is a corrective stereological factor to transform the 2D estimation (length per unit area) into a 3D estimation (surface per unit volume) assuming that the substructures pattern is repeated underneath the surface [29].

Thus, the equation (4) finally becomes:

$$E = \frac{\Delta}{S} \sum_i^N \gamma_{sub}(\theta_i) \quad (6)$$

The major drawback of this method is that only the dislocations forming subboundaries are considered. However, since the dislocations with small cumulative effect are not detected by EBSD, it can be reasonably assumed that this method is more suitable for the estimation of the stored energy from EBSD data. This method has nevertheless some limits of application for the case of low strains or the case of grains forming very few substructures.

Results and discussion

The two proposed methods were applied on the data estimated from EBSD maps acquired at the polycrystalline scale (step size of 1.20 µm) and at the substructure scale (step size of 90 nm). The estimated stored energies obtained with the two methods at the polycrystalline scale and at the substructure scale are presented in Table 2.

Table 2 Recrystallized fractions and values of stored energy estimated on the deformed state at the polycrystalline scale and at the substructure scale with the two methods.

Deformation condition	Annealing time at 850°C (h)	Recrystallized fraction (%)	Stored energy estimated on the deformed state (MJ/m^3)			
			Method based on dislocation density		Method based on dislocation substructures	
			Polycrystalline scale	Substructure scale	Polycrystalline scale	Substructure scale
Compression $\varepsilon_{VM} \approx 0.65$	1	5	3.0	8.1	0.64	0.79
	2	32				
	3	77				

Rolling $\varepsilon_{VM} \approx 1.67$	1	22	5.0	4.9	0.51	0.26
	2	35				
	3	62				

There is a significant difference between the stored energies estimated with the two methods. Several reasons could explain this discrepancy. Since the interactions between the energy field of the dislocations are roughly considered with the method based on equation (1), the stored energy is overestimated. On the other hand, the contribution of the measurement noise of EBSD data would increase the estimated dislocation density [25] and this distinguishes the two methods since only disorientation angles higher than 1.5° are considered in the second method.

Unlike the second method, the first method seems to give contradictory results depending on the observation scale: it increases with strain at the polycrystalline scale and decreases at the substructure scale. As discussed in recent studies [30,31], the choice of the step size has a significant influence on the estimated dislocation density. Only a part of the GNDs is detected when the step size is not chosen at the substructure scale. This indicates that only an arbitrary part of GNDs is estimated with EBSD data at the polycrystalline scale, unlike the estimation using EBSD data at the substructure scale (which is the main reason for which the dislocation density was termed $\overline{\rho_{EBSD}}$ and was not associated to GNDs). Hence, the estimated stored energy with the first method (equation (1)) cannot predict the recrystallization kinetics.

Even when GNDs are correctly estimated, i.e. at the substructure scale, GND density does not seem to be the appropriate parameter to predict recrystallization. In Fig.6, two micrographs with their associated EBSD maps at the substructure scale are presented. $\overline{\rho_{EBSD}}$ was estimated for the two cases and this value is supposed to be very close to the GND density at this scale. $\overline{\rho_{EBSD}}$ obtained for the γ-fiber grain (3.3×10^{15} m^{-2} as illustrated in Fig.6a) is lower than the one obtained for the θ-fiber grain (3.5×10^{15} m^{-2} as illustrated in Fig.6b). However, it would be expected that the γ-fiber grain would recrystallize faster because of the well-defined subboundaries unlike the θ-fiber grain. It could also be observed that the macroscopic plastic strain cannot be representative of the recrystallized fraction.

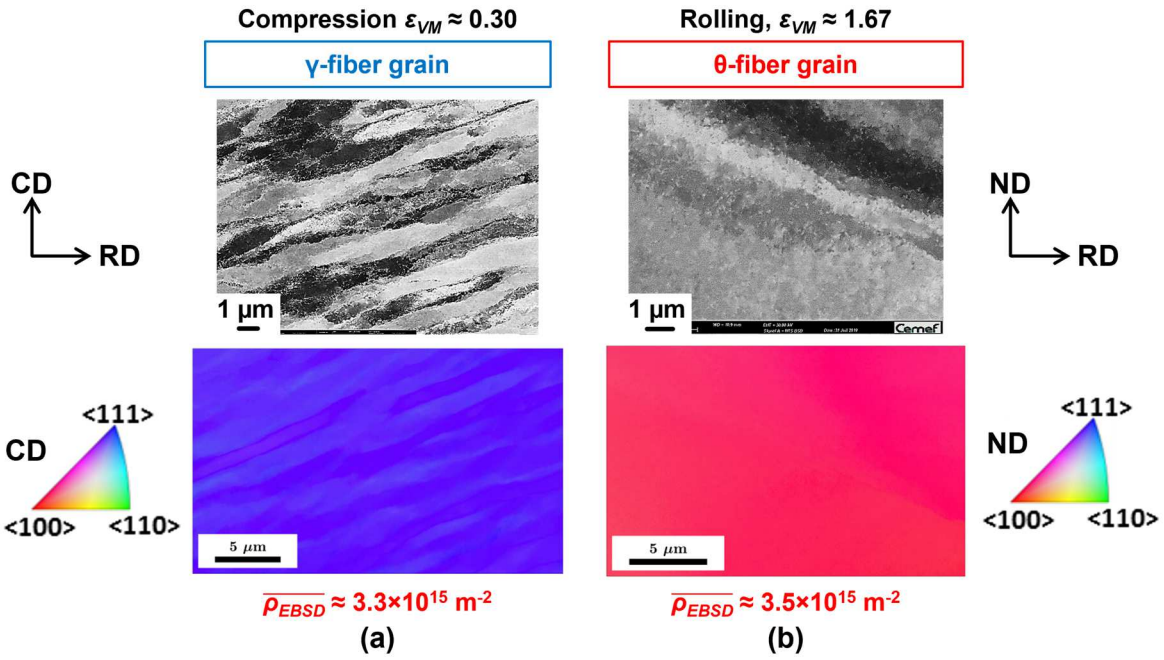

Fig.6 Micrographs obtained with the Electron Channeling Contrast Imaging (ECCI) technique and associated EBSD orientation maps acquired in the interior of (a) a γ-fiber grain in the microstructure of a compressed sample ($\varepsilon_{VM} \approx 0.30$) and (b) a θ-fiber grain in the microstructure of a rolled sample ($\varepsilon_{VM} \approx 1.67$) (CD and ND projected onto the standard triangle respectively).

For the case of the annealing for 3h, a correlation between the stored energy estimated with subboundaries and the recrystallized fraction is observed (higher stored energy leads to higher recrystallized fraction in Table 2). However, this correlation is not observed for the annealing for 1h and 2h. The main reason behind this observation is that, for the rolling case, and because of the high reduction, the number of grain boundaries (0.17 µm/µm²) is more than two times higher than for the compression case (0.07 µm/µm²). Unless grain boundaries are considered in the estimation of the stored energy, this parameter cannot be representative of the recrystallization kinetics since grain boundaries are the main nucleation sites.

One of the main conclusions is that a combination of the two methods at the substructure scale would be necessary in order to consider the two natures of dislocation distributions within the different grains: the method based on dislocation density for grains which do not develop substructures (θ-fiber grains in the present case) and the method based on substructures for grains which develop substructures (γ-fiber grains in the present case). In

addition, the number of grain boundaries would be considered because they are potential nucleation sites.

7. Conclusion

In this study, two different initial states of pure tantalum were compressed and rolled at room temperature. These two deformed samples were then annealed in order to investigate the influence of the deformed state on recrystallization. Recrystallization kinetics were then analyzed through the estimation of the stored energy at different scales. The main conclusions that can be drawn are:

- The plastic deformation of a grain considerably depends on its crystallographic orientation. In particular, the development of dislocation substructures is the highest in the γ-fiber grains and almost no substructure development is observed in θ-fiber grains.
- The orientation dependence of the deformed state inevitably impacts recrystallization: nucleation is enhanced in the γ-fiber grains due to the dislocation substructures whereas nucleation is slower in the θ-fiber grains due to the near absence of substructures.
- Microstructure composed mostly of γ-fiber grains, recrystallized faster than the one with a less pronounced texture, despite a strain nearly three times lower.
- For the estimation of the stored energy from EBSD data acquired at the polycrystalline scale (step size of 1.20 µm in the present case), the method based on substructures makes it possible to better account for the recrystallization kinetics than the method based on dislocation density.
- When the substructure scale is considered, it seems that the GND density may be estimated correctly. However, even at this scale, this density cannot account for the recrystallization kinetics since it does not account for the dislocation substructure formation. In additions, the grain boundary amount should be considered for recrystallization kinetics predictions.

Acknowledgments

The authors thank Cyrille Collin for the sample preparation, Gilbert Fiorucci for the mechanical tests and Suzanne Jacomet for the microscopy characterizations. The authors are also very thankful to CEA DAM Valduc for funding.

Conflict of interest

The authors declare that they have no conflicts of interest.

Data availability

The raw/processed data required to reproduce these findings cannot be shared at this time as the data also forms part of an ongoing study.

References

[1] Cardonne SM, Kumar P, Michaluk CA, Schwartz HD (1995) Tantalum and its alloys. Int J Refract Met Hard Mater 13:187–94. https://doi.org/10.1016/0263-4368(95)94023-R

[2] Jiang J, Britton TB, Wilkinson AJ (2015) The orientation and strain dependence of dislocation structure evolution in monotonically deformed polycrystalline copper. Int J Plast 69:102–17. https://doi.org/10.1016/j.ijplas.2015.02.005

[3] Baton J, Geslin W, Moussa C (2021) Orientation and deformation conditions dependence of dislocation substructures in cold deformed pure tantalum. Mater Charact 171:1–17. https://doi.org/10.1016/j.matchar.2020.110789

[4] Zhu L, Seefeldt M, Verlinden B (2013) Three Nb single crystals processed by equal-channel angular pressing—Part I: Dislocation substructure. Acta Mater 61:4490–503. https://doi.org/10.1016/j.actamat.2013.04.018

[5] Liu Y, Liu S, Lin N, Zhu J, Deng C, Liu Q (2020) Effect of strain path change on the through-thickness microstructure during tantalum rolling. Int J Refract Met Hard Mater 87:105168. https://doi.org/10.1016/j.ijrmhm.2019.105168

[6] Sandim HRZ, Padilha AF, Randle V, Blum W (1999) Grain subdivision and recrystallization in oligocrystalline tantalum during cold swaging and subsequent annealing. Int J Refract Met Hard Mater 17:431–5. https://doi.org/10.1016/S0263-4368(99)00035-9

[7] Baton J, Geslin W, Moussa C (2021) Influence of pre-recovery on the recrystallization of pure tantalum. J Mater Sci 56:15354–78. https://doi.org/10.1007/s10853-021-06218-0

[8] Primig S, Leitner H, Knabl W, Lorich A, Stickler R (2012) Static Recrystallization of Molybdenum After Deformation Below 0.5*TM (K). Metall Mater Trans A 43:4806–18. https://doi.org/10.1007/s11661-012-1292-4

[9] Deng C, Liu S, Hao XB, Ji JL, Zhang Z, Liu Q (2014) Orientation dependence of stored energy release and microstructure evolution in cold rolled tantalum. Int J Refract Met Hard Mater 46:24–9. https://doi.org/10.1016/j.ijrmhm.2014.05.005

[10] Borbély A, Driver JH, Ungár T (2000) An X-ray method for the determination of stored energies in texture components of deformed metals; application to cold worked ultra high purity iron. Acta Mater 48:2005–16. https://doi.org/10.1016/S1359-6454(99)00457-7

[11] Humphreys FJ, Hatherly M Recrystallization and Related Annealing Phenomena 2nd Edition. Elsevier; 2004

[12] Moussa C, Bernacki M, Besnard R, Bozzolo N (2015) About quantitative EBSD analysis of deformation and recovery substructures in pure Tantalum. IOP Conf Ser Mater Sci Eng 89:1–7. https://doi.org/10.1088/1757-899x/89/1/012038

[13] Moussa C, Bernacki M, Besnard R, Bozzolo N (2017) Statistical analysis of dislocations and dislocation boundaries from EBSD data. Ultramicroscopy 179:63–72. https://doi.org/10.1016/j.ultramic.2017.04.005

[14] Read WT, Shockley W (1950) Dislocation Models of Crystal Grain Boundaries. Phys Rev 78:275–89. https://doi.org/10.1103/PhysRev.78.275

[15] Godfrey A, Mishin OV, Yu T (2015) Characterization and influence of deformation microstructure heterogeneity on recrystallization. IOP Conf Ser Mater Sci Eng 89:1–19. https://doi.org/10.1088/1757-899X/89/1/012003

[16] Hull D, Bacon DJ Introduction to Dislocations (Fifth Edition). Oxford: Butterworth-Heinemann; 2011. https://doi.org/10.1016/C2009-0-64358-0

[17] Taheri M, Weiland H, Rollett A (2006) A method of measuring stored energy macroscopically using statistically stored dislocations in commercial purity aluminum. Metall Mater Trans A 37:19–25. https://doi.org/10.1007/s11661-006-0148-1

[18] Deng S-Q, Godfrey A, Liu W (2016) Analysis of Stored Energy in Cold-Rolled Copper Using Bulk and Microstructure-Based Techniques. Acta Metall Sin Engl Lett 29:313–9. https://doi.org/10.1007/s40195-016-0389-y

[19] Knudsen T, Cao WQ, Godfrey A, Liu Q, Hansen N (2008) Stored Energy in Nickel Cold Rolled to Large Strains, Measured by Calorimetry and Evaluated from the

Microstructure. Metall Mater Trans A 39:430–40. https://doi.org/10.1007/s11661-007-9421-1

[20] Hazra SS, Gazder AA, Pereloma EV (2009) Stored energy of a severely deformed interstitial free steel. Mater Sci Eng A 524:158–67. https://doi.org/10.1016/j.msea.2009.06.033

[21] Bachmann F, Hielscher R, Schaeben H (2011) Grain detection from 2d and 3d EBSD data—Specification of the MTEX algorithm. Ultramicroscopy 111:1720–33. https://doi.org/10.1016/j.ultramic.2011.08.002

[22] Wilkinson AJ Deformation Textures.In: Buschow KHJ, Cahn RW, Flemings MC, Ilschner B, Kramer EJ, Mahajan S, Veyssière P, editors.Encycl. Mater. Sci. Technol., Oxford: Elsevier; 2001, p. 2022–6. https://doi.org/10.1016/B0-08-043152-6/00368-5

[23] Raabe D, Schlenkert G, Weisshaupt H, Lücke K (1994) Texture and microstructure of rolled and annealed tantalum. Mater Sci Technol 10:299–305. https://doi.org/10.1179/mst.1994.10.4.299

[24] Pantleon W (2008) Resolving the geometrically necessary dislocation content by conventional electron backscattering diffraction. Scr Mater 58:994–7. https://doi.org/10.1016/j.scriptamat.2008.01.050

[25] Seret A, Moussa C, Bernacki M, Signorelli JW, Bozzolo N (2019) Estimation of geometrically necessary dislocation density from filtered EBSD data by a local linear adaptation of smoothing splines. J Appl Crystallogr 52:548–63. https://doi.org/10.1107/S1600576719004035

[26] Lin N, Liu S, Liu Y, Fan H, Zhu J, Deng C, Liu Q (2019) Effects of asymmetrical rolling on through-thickness microstructure and texture of body-centered cubic (BCC) tantalum. Int J Refract Met Hard Mater 78:51–60. https://doi.org/10.1016/j.ijrmhm.2018.08.012

[27] Jafari M, Jamshidian M, Ziaei-Rad S, Raabe D, Roters F (2017) Constitutive modeling of strain induced grain boundary migration via coupling crystal plasticity and phase-field methods. Int J Plast 99:19–42. https://doi.org/10.1016/j.ijplas.2017.08.004

[28] Cao WQ, Godfrey A, Liu Q (2003) EBSP investigation of microstructure and texture evolution during equal channel angular pressing of aluminium. Mater Sci Eng A 361:9–14. https://doi.org/10.1016/S0921-5093(03)00055-8

[29] Underwood EE Quantitative Stereology for Microstructural Analysis.In: McCall JL, Mueller WM, editors.Microstruct. Anal. Tools Tech., Boston, MA: Springer US; 1973, p. 35–66. https://doi.org/10.1007/978-1-4615-8693-7_3

493 [30] Ruggles TJ, Rampton TM, Khosravani A, Fullwood DT (2016) The effect of length
494 scale on the determination of geometrically necessary dislocations via EBSD continuum
495 dislocation microscopy. Ultramicroscopy 164:1–10.
496 https://doi.org/10.1016/j.ultramic.2016.03.003
497 [31] Naghdy S, Verleysen P, Petrov R, Kestens L (2018) Resolving the geometrically
498 necessary dislocation content in severely deformed aluminum by transmission Kikuchi
499 diffraction. Mater Charact 140:225–32. https://doi.org/10.1016/j.matchar.2018.04.013
500